Proceedings of ICFDP7:
Seventh International Congress on Fluid Dynamics and Propulsion
December 18-20, 2001, Cairo, Egypt

ICFDP7-2001070

A STUDY ON HIGH-SPEED PULSATING JET

Atsunori Kimura and Junjiro Iwamoto

Tokyo Denki University, 2-2 Kanda-Nishiki-cho, Chiyoda-Ku. Tokyo 101-8457 Japan.

ABSTRACT

This paper describes the noise seen in an exhaust system of a reciprocating internal combustion engine. We focused on some jet noise in particular. The phenomena of high-speed pulsating flow through an exhaust pipe and the jet efflux into atmosphere were studied both experimentally and numerically. The experiment and calculation were conducted and simulated under various operating conditions of the engine. The comparison between the results in experiment and those in calculation showed good agreement. The noise sources appeared at the moment when the pulsating jet generated was examined. As the result of employing high accurate numerical scheme, it becomes clear that there are four noise sources , in the pulsating jet., a discharged shock wave, a vortex ring (vortex shedding sound), an interaction of the shock wave with the vortices and Mach wave radiation in an underexpanded jet.

INTRODUCTION

There are many engineering problems in developing an automobile, those problems being concerned with the reduction of exhaust gas including some poisonous substances, traffic noise, the improvement of fuel efficiency and so on. In other words it is demanded that the damage to environment should be controlled. From the viewpoint of fluid dynamics research, we are greatly interested in the reduction of the exhaust noise. The effort of study in this field has continued in order to clarify the relation between the flow behavior and the resultant noise. Moreover, the progress of the performance of a computer stimulated this field. Recently the establishment of TVD scheme in the area of numerical analysis has played an important role in clarifying it, so that it is found that the shock wave generated by the nonlinearity of the compression wave propagating through the exhaust pipe is now known to be one of the noise sources. The distortion of the propagating compression wave is essentially similar to that seen in a high-speed railway tunnel, or tunnel sonic boom [1]. It deserves our attention to use the initial gradient of the compression wave as a parameter in the research. That is because the gradient of the compression wave produced by the opening of the exhaust valve of an engine is easily expected to strongly depend on the operating conditions. For example, the gradient becomes steeper the shorter the opening time of the valve changes.

Some papers, which reported the noise seen in an internal combustion engine so far elsewhere, showed excellent results involved in the mechanism of the shock wave formation and its discharge. However it is true that the discharged shock wave is dominant noise source, but it is not always the one and only noise source as our research group has shown [2]. In fact in the flow field upstream of the discharged shock wave, a vortex ring and an underexpanded jet are formed. Subsequently, the flow field develops, and the vortex ring and the underexpanded jet are diffused as they move downstream. This flow pattern repeats itself periodically. For instance, it is well-known that the noise generated in an underexpanded jet which issues from a convergent nozzle steadily is caused by quadrupole sound predominantly. It appears that there are three types of the noise sources: monopole, dipole and quadrupole, those sound intensities (I_m, I_d, I_q, each subscript represents the initial letter of the word) being expressed in the following equations,

$$I_m \sim \rho_0 r_0^{-2} a_0^{-1} L^2 U_0^4 \tag{1}$$

$$I_d \sim \rho_0 r_0^{-2} a_0^{-3} L^2 U_0^6 \tag{2}$$

$$I_q \sim \rho_0 r_0^{-2} a_0^{-5} L^2 U_0^8 \tag{3}$$

where ρ_0, r_0, a_0, U_0, and L are the density, the distance from noise source, the sonic velocity in uniform flow, the velocity and the reference scale of a body. The ratios among them are,

$$\frac{I_d}{I_m} = \frac{I_q}{I_d} \sim \left(\frac{U_0}{a_0}\right)^2 = M_0^2 \tag{4}$$

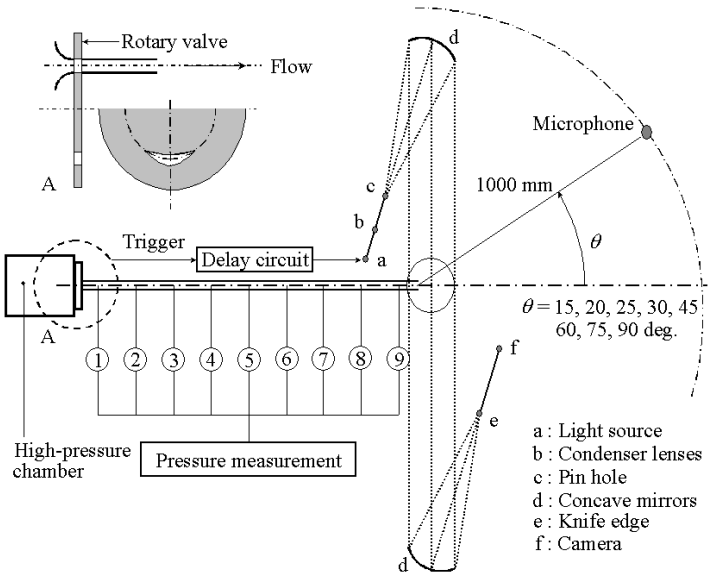

Figure 1. Experimental apparatus

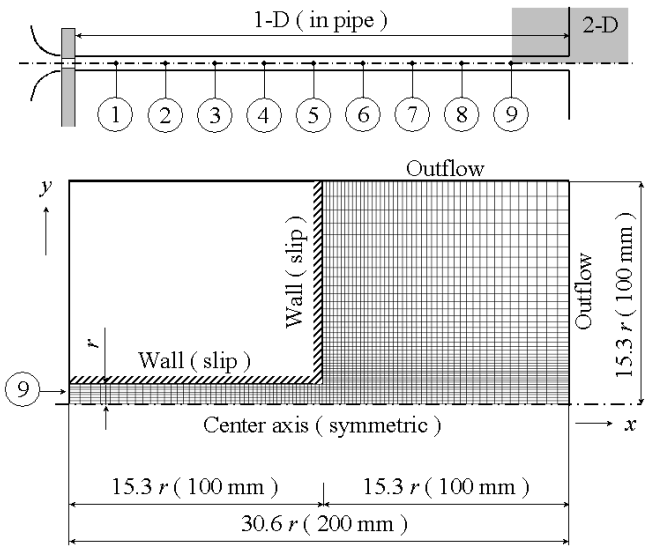

Figure 2. Computational domains

It is said that jet noise belongs to quadrupole sound. Therefore the jet noise appearing in the underexpanded jet following discharged shock wave can not be neglected since it has high Mach number.

In the present study, a variety of the noise generations and the flow behavior regarding the operating condition of an engine were explored by numerical simulation and experiment.

NOMENCLATURE

p_{atm} Atmospheric pressure
n Rotational speed of the rotary valve (rpm)
r Radius of the pipe (6.5 mm)
t Passed time from the moment when the rotary valve opens
t_d $t_d = 0$ means at the moment when the head of compression wave in the pipe exactly arrives at the pipe end
τ The time during one period of the rotary valve
x Axial distance, the origin is at the center of the pipe end
y Radial distance, the origin is at the center of the pipe end

EXPERIMENTAL SETUP

A schematic view of an experimental apparatus is shown in figure 1. Compressed air is supplied into the high-pressure chamber. The air flows into a 1m long straight pipe, whose internal diameter is 13mm, through the rotary valve so that a pulsating flow can be generated and the pulsating jet is discharged from the pipe end into atmosphere. There are two ports in the rotating disk (in figure 1, at "A"). The rotation and the overlapping between the port and the pipe make the flow pulsating into the pipe. The change of the opening area ratio of the port to the pipe is designed to be equal to that of an exhaust port of a typical internal combustion engine. The rotational speed of the disk, n, is adjustable arbitrarily. It should be noted that n = 3000rpm for example, it corresponds to 6000rpm of a real engine. The trigger signal is picked out sequentially at the moment when the rotary valve begins to open, that is, $t = 0$. Nine pressure ports exist along the pipe and the distances between neighboring ports are 100mm. The pulsating jet is visualized by shadowgraph method. The microphone placed in the sound proof room is used for sound pressure measurement at each location shown in figure 1. As to the experimental conditions, n changes from 1200 to 3300rpm at intervals of 300rpm and the pressure in the high-pressure chamber is kept at 4.0atm.

NUMERICAL SIMULATION

Figure 2 shows computational domains. As the pressure of sound which is audible is 20μ Pa ~ 20 Pa, the value of which is about 10^{-4} less than the flow pressure, high accuracy is required to capture both properties of flow and noise. Hence in order to avoid simultaneously treating the flow fields of both pulsating flow through the pipe and the jet in terms of keeping its accuracy, the numerical simulation was made by the coupling of two procedures: the flow field in the pipe was simulated by solving one-dimensional Euler equation and, using these results as the boundary condition, the simulation of the jet was carried out by solving a two-dimensional Euler equation under the assumption of axially-symmetric flow. For the former governing equation the convective term was

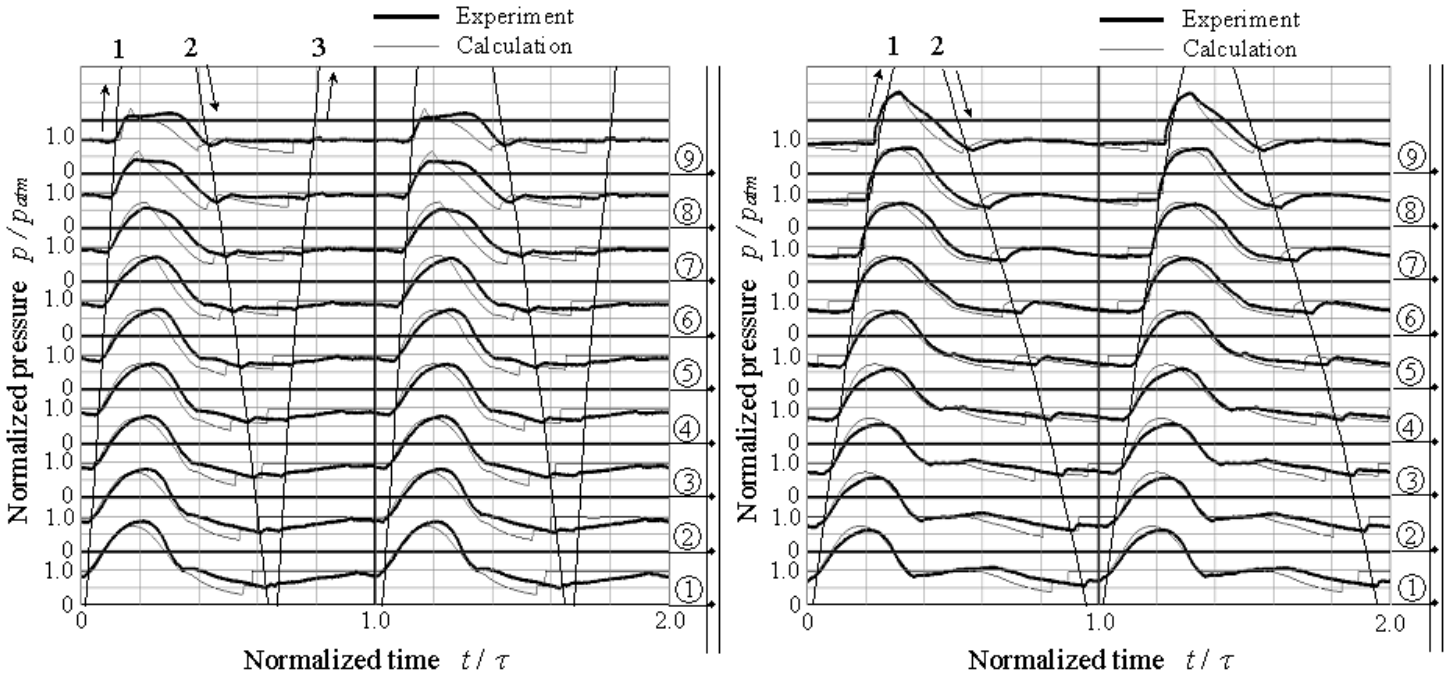

(a) n = 1500 rpm

(b) n = 3000 rpm

Figure 3. Pressure histories in the pipe

solved by a third order MUSCL TVD [3] scheme, while for the latter case a fifth order compact MUSCL TVD [4] scheme was employed where the properties both sides of a cell interface was evaluated by basing on the primitive variables. Using these values, numerical fluxes are estimated by Roe's approximate Riemann solver. A three-stage Runge-Kutta method was used for time integration.

In two-dimensional analysis 750 cells are used for discretization in the axial direction, and 350 cells in the radial direction. Regarding the mesh generation, it is very important to be sufficient to resolve the jet. Thus each grid is coagulated toward the location of shear layer and the pipe end.

RESULTS AND DISCUSSION

In this section, the relation between the flow field of the pulsating jet and the noise generation is primarily discussed. Since the behavior of the jet, however, is closely related to the flow field in the pipe, it will be discussed first.

Pressure Histories in the Pipe

Figure 3 shows the pressure histories in the pipe at n = 1500 and 3000rpm. Both the abscissa and the ordinate were normalized by p_{atm} and τ, respectively. Each curve expressing the pressure history was measured at each location illustrated in the right side of the figure. The opening of the rotary valve produces 1st compression wave (1CPW) propagating downstream along a line numbered 1. Then expansion wave follows the 1CPW after the moment when the opening area of the rotary valve takes a critical value. The 1CPW is distorted by the effect of the nonlinearity in itself as it propagates downstream. The phenomenon of the wave distortion at n = 3000 rpm appears more conspicuous than that at n = 1500 rpm. Comparing between these cases of τ, that at n = 3000 rpm is half as long as that at n = 1500 rpm. Therefore the difference is caused by the initial gradient of 1CPW.

Second compression wave propagating upstream, which moves along a line numbered 2, is generated by the reflection of the expansion wave coupled with the 1CPW at the pipe end. Third compression wave appears after its reflection at the closed rotary valve only at n = 1500 rpm.

Regarding the comparison between the result in calculation and that in experiment, there are two discrepancies. One is the gradient at the head of the 1CPW. It appears that the gradient in the calculation is steeper than that in the experiment. The other is the reflection of 1CPW influencing the pressure curves at 8 , 9 and so on between the lines, 1 and 2. It is known that the incidence of a compression wave to an open end of a pipe makes an expansion wave. The former concerns the governing equation used in the present study, that is to say, this simulation was made under the assumption of frictionless and adiabatic. Hence the result is liable to leading to easy formation of shock wave. The latter

problem converges on the treatment of the boundary condition when the air flows out at the pipe end

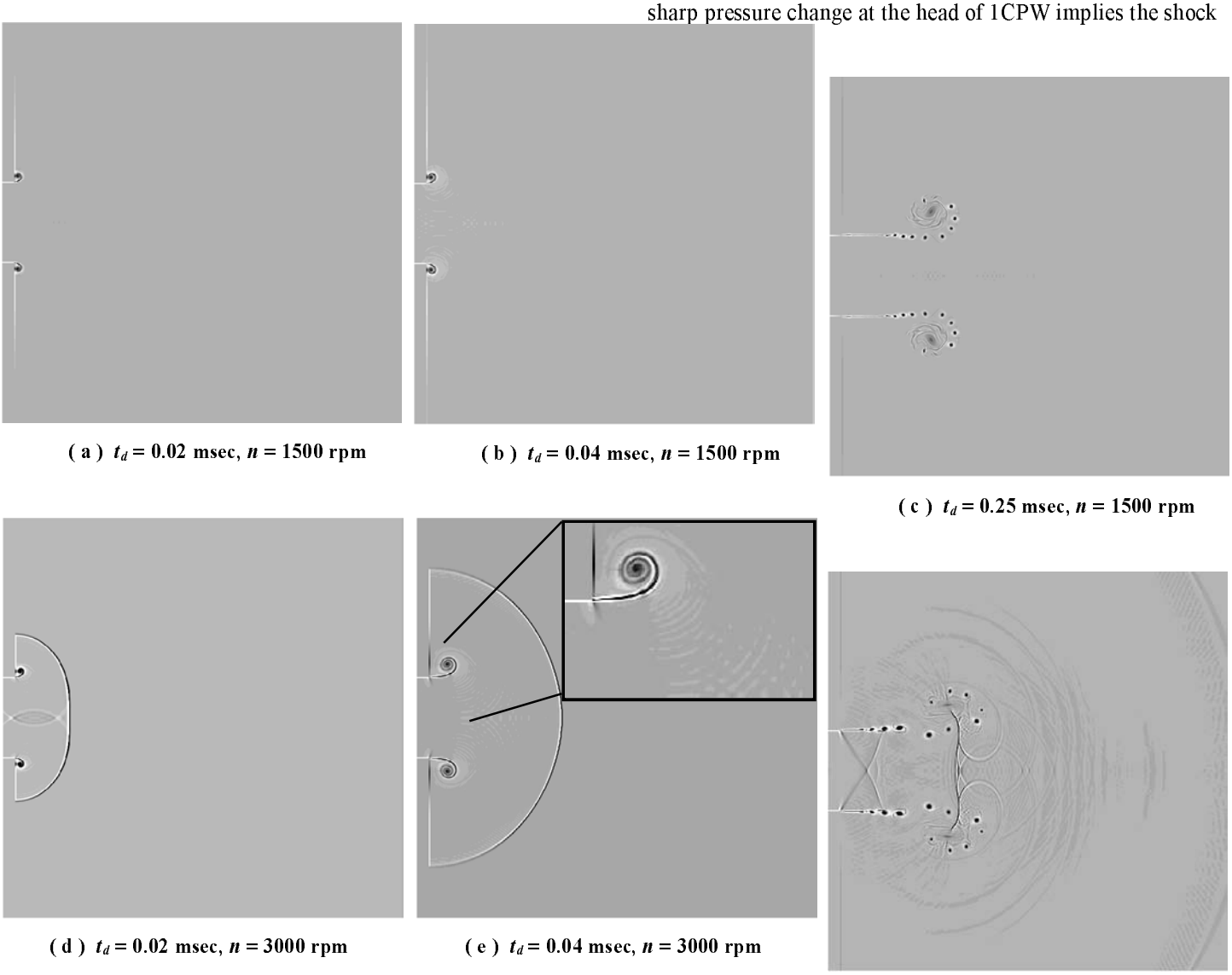

(a) t_d = 0.02 msec, n = 1500 rpm **(b) t_d = 0.04 msec, n = 1500 rpm** **(c) t_d = 0.25 msec, n = 1500 rpm**

(d) t_d = 0.02 msec, n = 3000 rpm **(e) t_d = 0.04 msec, n = 3000 rpm**

Figure 4. A series of computed shadowgraph photographs

subsonically. In the case of subsonic outflow, atmospheric conditions very often are imposed there. But it is not strictly reasonable on one dimensional computation because the flow behavior near the pipe end is considered to be three dimensional.

Flow Field of the Pulsating Jet

Figure 4 shows the computed shadowgraph photographs taken at n = 1500 and 3000 rpm. In these pictures a remarkable difference among them is firstly the existence of the discharged shock wave. There are no shock wave at n = 1500 rpm. It is found that the difference comes from each flow field in the pipe. As shown in figure 3 at n = 3000 rpm, the sharp pressure change at the head of 1CPW implies the shock The shock wave through the pipe is discharged from the open end, diffracted by the expansion wave generated simultaneously from the edge of the pipe end. This process can be seen in the picture taken at t_d = 0.02 msec and n = 3000 rpm. The pressure variation across the diffracted shock wave has a pulse-like form and it becomes one of the noise source seen in the pulsating jet.

The shock wave and the compression wave propagating downstream through the pipe in the present study induce the flow of air toward the same direction behind them. The influence of the shear stress of the atmosphere on the flow produces the vortex ring at the instant when it issues from the

pipe end. The vortex ring is observable in figure 4 (a) and (d), developing its structure as it rolls up the shear layer of the jet. In figure 4 (e) the vortex ring moves away from the pipe end and then very weak sound wave appears around it, while the sound wave is invisible in figure 4 (b). It appears that the appearance of the sound wave is connected with the change of the vorticity at the core of the vortex ring as shown in figure 5. The vorticity at n = 3000 rpm decreases by far more suddenly than that at n = 1500 rpm. The vortex shedding sound could be actually confirmed at speed over 1800 rpm, where the change of the vorticity has the same tendency as that at 3000 rpm.

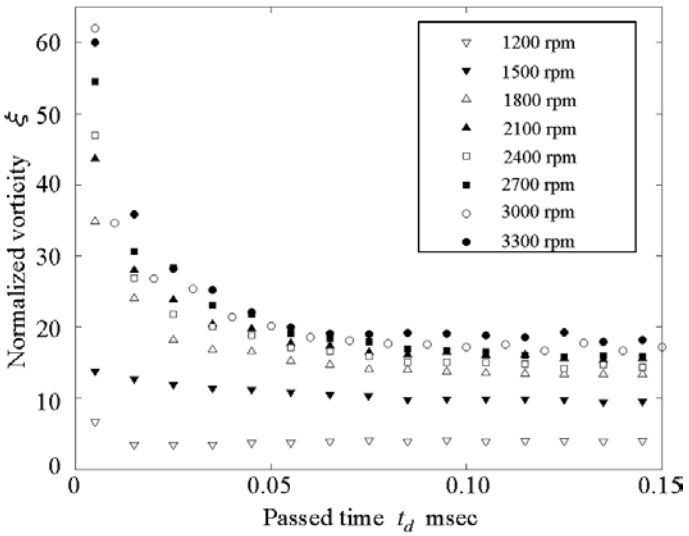

There are two different phenomena between figure 4 (c) and 4 (f). One is whether or not the shock wave between the vortex cores generates. It is widely understood that the formation of the shock wave has the same mechanism as that in a convergent and divergent (CD) nozzle flow. The vortex sheet rolling the vortex core plays a role as the throat of a CD nozzle. The shock wave appears, provided that the relative velocity between the convective velocity of the vortex ring and the speed of the flow passing through the vortex ring is sonic, namely, the flow chokes. It is interesting that the cellular structure of the underexpanded jet is visible behind the vortex ring only in figure 4 (f). That is because the appearance implies the relative velocity becomes higher than that in figure 4 (c).

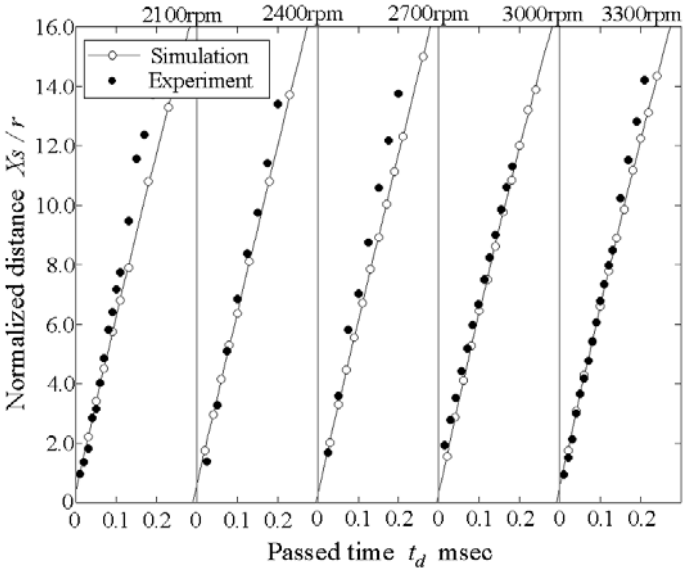

Figure 6. Locations of the discharged shock wave

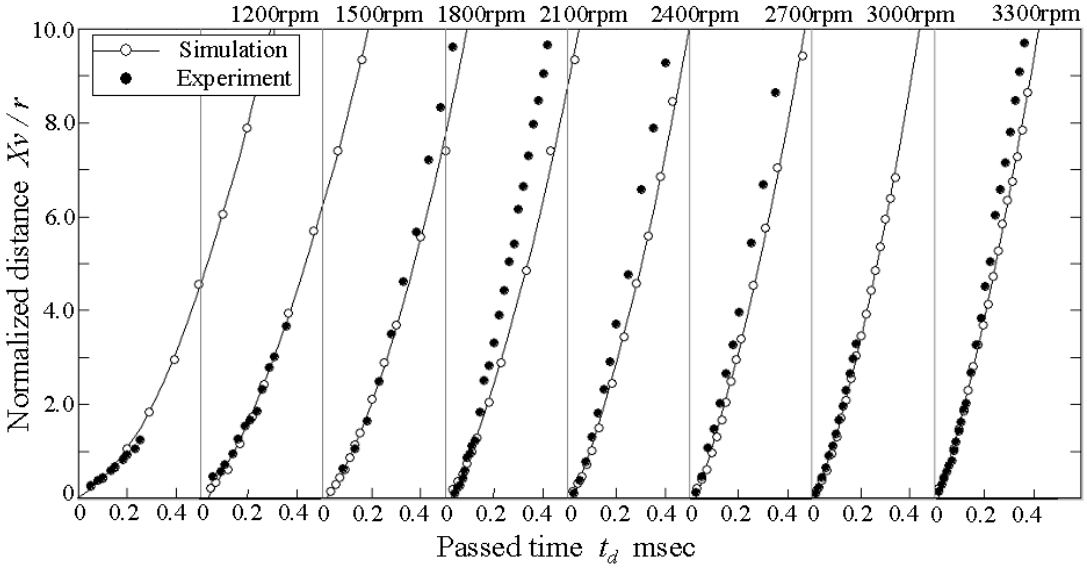

Figure 7. Locations at the core of the vortex ring

This will be fully discussed in later section. The other difference is sound waves traveling downstream of the vortex ring in figure 4 (f). The rolled-up vortices which the Kelvin-Helmholtz instability of the jet shear layer produces successively move downstream, and scattered waves are spherically radiated by the result of the interaction between the vortices and the shock wave in the vortex ring. On the other hand the waves are not produced at n = 1500 rpm because of no shock wave in the vortex ring. The flow field in the present study is very similar to that produced in a shock tube. However, there are no papers published on the same phenomenon in the area of shock tube flow as far as the authors are aware. The pulsating flow through the pipe essentially differs from that of a shock tube in terms of the presence of the shock wave followed by compression wave. The reflection of the compression wave at the open end makes the expansion wave propagating upstream, so that the flow in the vicinity of the pipe end is accelerated even higher. As a result, it is supposed that the convective velocity of the vortices increases and they can interact with the shock wave easily.

In figures 6 and 7 the comparisons of the experimental result with the simulation are shown, where X_s and X_v denote the axial distance of the discharged shock wave and the location of the vortex ring from the pipe end, respectively. The discharged shock wave comes into existence beyond n = 2100 rpm, while the vortex ring exists over the whole speed range of the rotary valve. In figure 6 its velocity depends on the jet strength near the open end, but after the jet blast it approaches asymptotically a sonic velocity. In figure 7 the results obtained by the simulation agree with the experiment near the pipe end, but it is because the vortex core becomes difficult to identify at far distance that the discrepancies expand as the convection of the vortex ring advances. It is noticeable that each convective velocity of the vortex ring takes a constant value as time goes by.

Shock / vortex interaction

As mentioned in the previous section, the detailed information of the interaction of the shock wave in the vortex

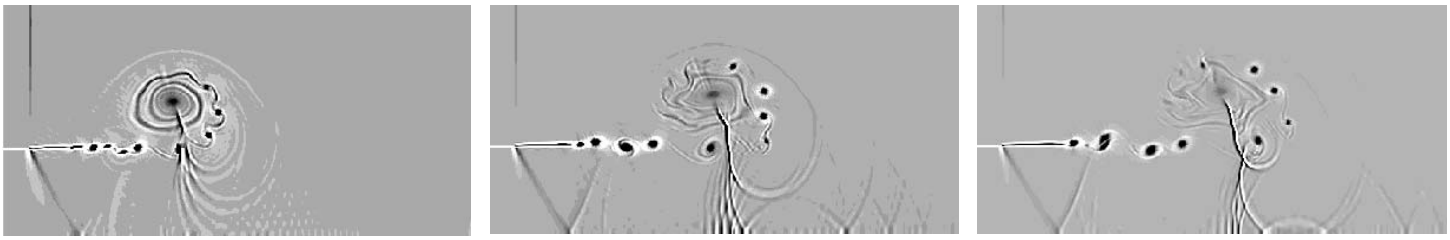

Figure 8. Shock / vortex interaction at t_d = 0.12, 0.15 and 0.16 msec (n = 3000 rpm)

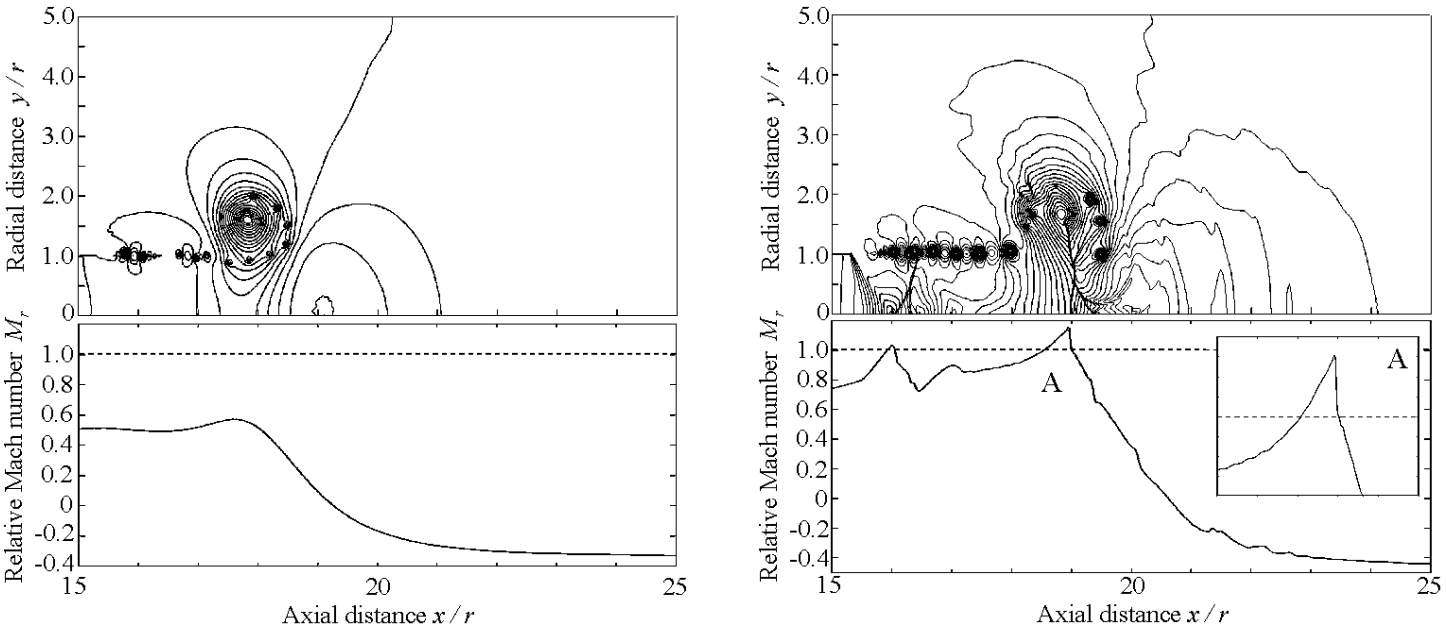

(a) n = 1500 rpm at t_d = 0.27 msec **(b) n = 3000 rpm at t_d = 0.20 msec**

Figure 9. The relation between the shock wave generation and the relative Mach number

ring with the vortices is shown in figure 8. At t_d = 0.12 msec the shock wave begins to form from the vortex core, and some comparatively weak waves are produced at that time when the vortices interacts with the shocklet. It is found that, as shown later, the flow field through the vortex ring chokes because those waves no longer propagate upstream at t_d = 0.15 msec. Hence, the sound waves are considered to have the directivity toward the jet axis.

A relative Mach number, M_r, is defined before the explanation of figure 9. The M_r is expressed in the following equation,

$$M_r = \frac{v_j - v_{vor}}{c_l} \tag{5}$$

where v_j is the local velocity at the jet axis, v_{vor} the convective velocity of the vortex ring derived from the result in figure 7 and c_l the local speed of sound at the jet axis; i.e. the property, M_r, represents the relative Mach number between the moving vortex ring and the flow passing through it. Hence, it is useful to introduce M_r for investigation of CD nozzle flow. Figure 9 shows the pressure contours (upper half) and the relative Mach number distributions (lower half). At n = 1500 rpm the air flow across the vortex ring remains subsonic, while there is supersonic region at n = 3000 rpm. The flow behind the vortex ring is gradually accelerated toward it, and M_r becomes greater than 1. Then the flow becomes supersonic finally, and M_r decreases suddenly at the location where the shock wave in the vortex ring generates. In these circumstances the flow field corresponds to that of CD nozzle. It is concluded that the reason for the generation of the shock wave in the vortex ring consists in, so-called, CD nozzle effect.

Mach wave emission

It is generally well known that a supersonic jet which exhausts into atmosphere steadily generates a noise known as Mach wave emission. The mechanism is due to the acceleration motion of roll-up vortex in the downstream direction and the roll-up vortex produced in jet shear layer is

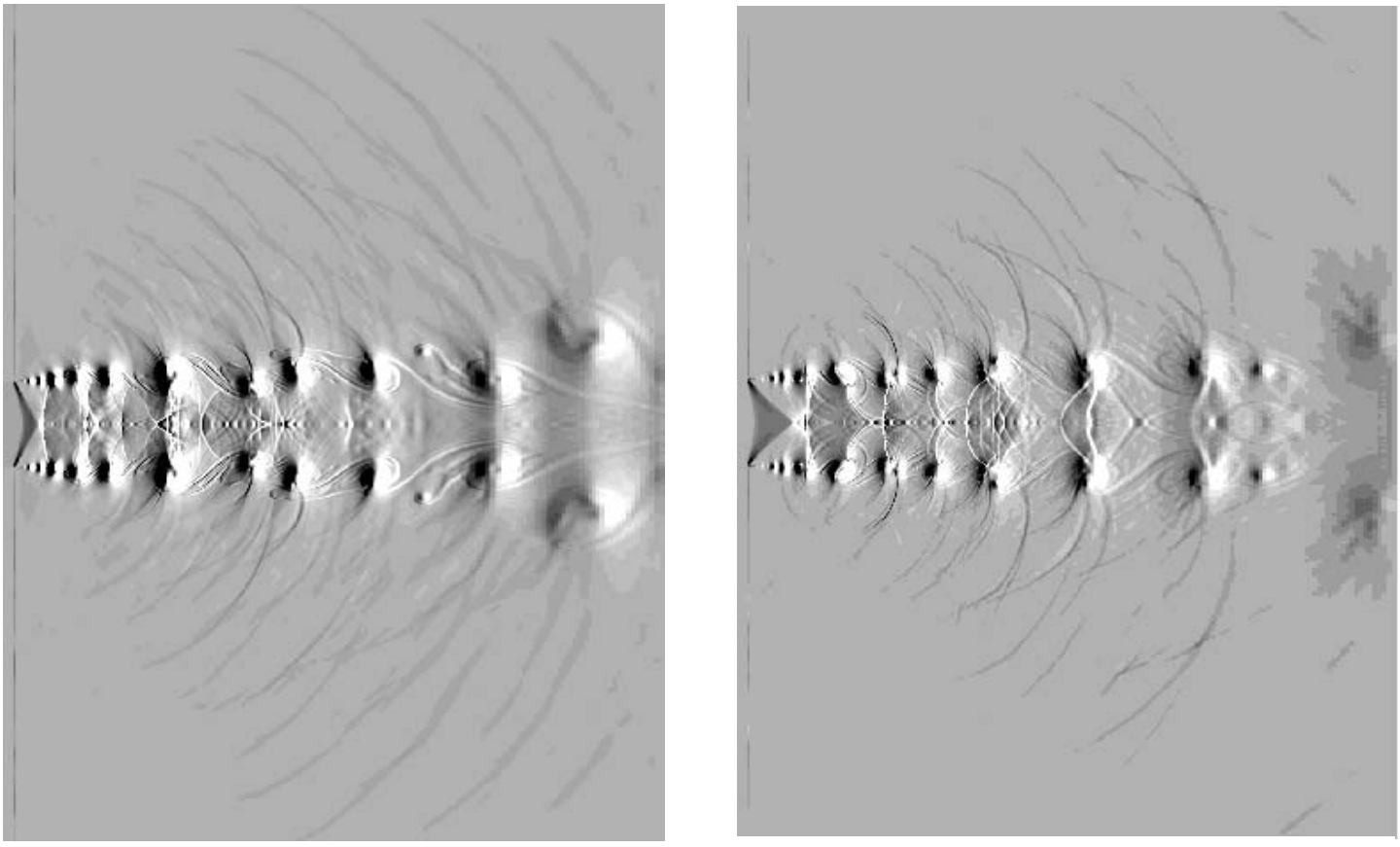

Figure 10. Mach wave emission from the underexpanded jet with using computed schlieren method

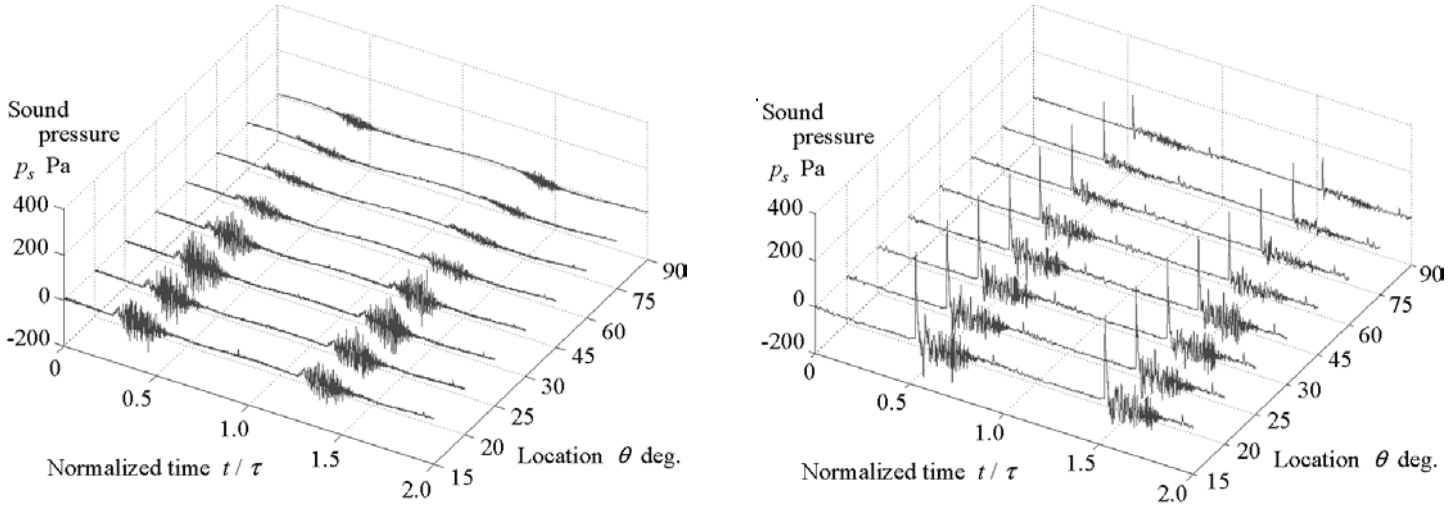

(a) n = 1500 rpm **(b) n = 3000 rpm**

Figure 11. Sound pressure histories

of quadrupole [5]. In the present study the flow rate at the pipe end changes with time, but Mach wave emission is clearly seen in figure 10. The axial width between adjacent vortices becomes large downstream due to acceleration motion of the vortices.

Sound pressure histories

Figure 11 shows sound pressure histories measured at each location illustrated in figure 1. The spike-like waves at n = 3000 rpm are generated by the discharged shock wave. It is obvious that the sound pressure histories at n = 1500 and 3000 rpm has directivity, especially from 15 to 45 degrees. In the viewpoint of the directivity the sound pressure histories at n = 1500 rpm and that behind the spike-like wave at n = 3000 rpm are induced by either only Mach wave emission or the combination in the noise produced by the shock/vortex interaction with Mach wave emission shown in figure 8 and 10, respectively.

CONCLUDING REMARKS

In order to analyze the mechanism of the noise generation from the pulsating flow field downstream of the exhaust pipe end, numerical and experimental studies were carried out. Table 1 shows the relation between the flow field and the noise obtained in the present study as regards the speed of the rotary valve. The exhaust noise seen in an automobile is roughly classified into monopole sound. However, it becomes clear that the noise examined in further detail can be divided into some elements. The discharged shock wave has already been known

Table 1. Flow field of the pulsating jet

n rpm	1200	1500	1800	2100	2400	2700	3000	3300
Underexpanded jet	existence							
Vortex ring								
Discharged shock	non existence							
Shock in vortex ring								
Vortex shedding sound								
Shock/vortex interaction								
Mach wave emission								

REFERENCES

[1] Fukuda, T., Iida, M., Maeda, T., Maeno, K., and Honma, H., 1998, "Investigation of Compression Wave Propagating in Slub Tunnel of High-Speed Railway", JSME(B), Vol. 64, No. 621, pp. 107-113.

[2] Endo, M., and Iwamoto, J., 1999, "A Study of Pulsatile Jet Discharged from Pipe End", J. of Visualization, Vol. 1, No. 3, pp. 261-269.

[3] Yee, H.C., 1989, "A Class of High Resolution Explicit and Implicit Shock-Capturing Methods", NASA TM-101088, pp. 1-218.

[4] Yamamoto, S., 1999, "SHOCK-VORTEX CAPTURING METHOD AND ITS APPLICATION TO UNSTEADY 3-D CASCADE FLOW", CFD JOURNAL, Vol. 8, No. 2, pp. 341-349.

[5] Nakamura, Y., and Yamaguchi, H., 1999, "COMPRESSIBLE JET AND ITS SOUND EMISSION", CFD JOURNAL, Vol. 8, No. 2, pp. 250-256.